Concurrent Structure and Process Optimization for Minimum Cost Metal Additive Manufacturing

Erva Ulu, Runze Huang, Levent Burak Kara, Kate S. Whitefoot[*]
Department of Mechanical Engineering
Carnegie Mellon University
Pittsburgh, Pennsylvania 15213
Email: kwhitefoot@cmu.edu

Metals-additive manufacturing (MAM) is enabling unprecedented design freedom and the ability to produce significantly lighter weight parts with the same performance, offering the possibility of significant environmental and economic benefits in many different industries. However, the total production costs of MAM will need to be reduced substantially before it will be widely adopted across the manufacturing sector. Current topology optimization approaches focus on reducing total material volume as a means of reducing material costs, but they do not account for other production costs that are influenced by a part's structure such as machine time and scrap. Moreover, concurrently optimizing MAM process variables with a part's structure has the potential to further reduce production costs. This paper demonstrates an approach to use process-based cost modeling in MAM topology optimization to minimize total production costs, including material, labor, energy, and machine costs, using cost estimates from industrial MAM operations. The approach is demonstrated on various 3D geometries for the electron beam melting (EBM) process with Ti64 material. Concurrent optimization of the part structures and EBM process variables are compared to sequential optimization, and to optimization of the structure alone. The results indicate that, once process variables are considered concurrently, more cost effective results can be obtained with similar amount of material through a combination of (1) building high stress regions with lower power values to obtain larger yield strength and (2) increasing the power elsewhere to reduce the number of passes required, thereby reducing build time. In our case studies, concurrent optimization of the part's structure and MAM process parameters lead to up to 15% lower estimated total production costs and 21% faster build time than optimizing the part's structure alone.

1 Introduction

Metals-additive manufacturing (MAM) has the potential to offer unprecedented design freedom by allowing complex geometries to be created that are impossible or cost pro-

hibitive to produce through traditional manufacturing methods [1]. It is also enabling the production of significantly lighter weight parts with the same performance, offering the possibility of significant environmental and economic benefits in many industries, including aerospace, medical, and energy [1–3]. However, relatively high production costs of MAM are preventing widespread adoption across many manufacturing sectors [1,4]. Studies have demonstrated that optimizing the structural design of MAM parts can help decrease material usage, and therefore material costs, while maintaining part performance [5–7]. The classic topology optimization formulation minimizes compliance or stress subject to a constraint on the total volume [8–11], representing a proxy for material costs [12–16]. However, a part's topology also influences production costs through means other than the costs associated with the material contained in the final part. For example, scrap and energy costs depend on where exactly material in the machine build envelope is added to a part and where it is not [4]. Furthermore, MAM process variables, such as laser/beam power and speed, influence production costs associated with machine time and energy as well as material properties [17]. Concurrent optimization of MAM process variables and a part's topology therefore has the potential to further reduce the production costs. While the potential to optimize AM process parameters and part topology has been discussed in the literature [18,19] and empirical case studies have been presented to optimize process parameters given a fixed topology [20–25], no previous literature has concurrently optimized a part's topology as well as process variables. Moreover, no existing methodologies have been developed to minimize total production costs in a topology optimization, which, as we discuss, can lead to significantly different part designs than the standard topology optimization formulation.

In this paper, we demonstrate a production cost minimization approach for MAM that concurrently optimizes the part structure and process variables, including beam power and velocity (Figure 1). The approach is developed by integrating efficient topology optimization, process-based cost modeling (PBCM), and MAM process/solidification map-
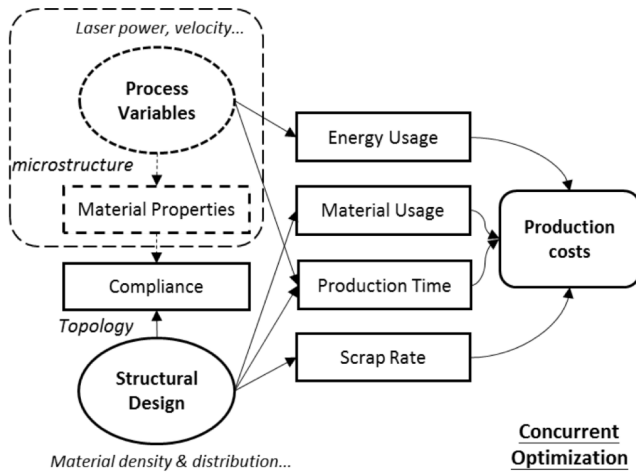

Fig. 1. Cost minimization framework. The dashed lines contain the elements included in the concurrent optimization but not the optimization of structural design alone.

ping between process variables and microstructure. The main focus of the paper is to present the methodology and demonstrate that accounting for the influence of both structural design and MAM process parameters on total production costs can lead to different design topology solutions that have similar material usage but lower total production costs compared to solely optimizing the structure.

2   Related Work

We draw on three different methods to develop the methodology presented in this paper: topology optimization, process-based cost modeling, and process mapping for MAM. This section describes these methods and reviews past work relevant to additive manufacturing (AM).

2.1   Topology Optimization

Due to the unique capabilities of AM, new methods and tools are needed to improve design for AM (DFAM) to maximize product performance [26]. One class of methods ripe for adaptation for DFAM is topology optimization—a powerful technique in structural design that optimizes the shape and material connectivity of a domain through the use of finite element methods together with various optimization techniques [8, 27]. Topology optimization has been extensively applied for designing AM parts [13, 14, 19, 28]. Recent adaptations of topology optimization for DFAM include considering the constraints of support structures [15], internal patterns [29], as well as applications in design of cellular structures [30], heat sinks [16], and tissue scaffolds [7]. However, these approaches do not consider the influence of structural design on total AM production costs or the significance of process variables in reducing these costs.

Density-based topology optimization approaches are one of the well studied methods in the literature [11, 31, 32]. These methods approach the design problem in a way that the structure is defined by optimizing the material distribution

in the domain. Since each finite element within the design domain is defined as a design variable, these methods provide extensive flexibility in allowing the resulting geometry to be highly complex. The objectives of most existing topology optimization approaches for AM, however, are limited to minimizing the compliance, or maximizing the strength of the structure [33]. In this paper, on the other hand, we focus on minimizing the overall production cost with respect to the element densities as well as the MAM process variables.

2.2   Cost Modeling

A variety of studies have been conducted to identify the main factors that influence AM production costs. Thomas et al. performed a literature review of economic studies and cost models of polymeric and metallic AM processes [4]. Hopkinson and Dickens analyzed the costs of polymeric AM and compared them with the cost of injection molded parts [34]. Similarly, the economic efficiency of MAM methods including selective laser sintering and selective laser melting have been compared against conventional manufacturing methods [35, 36]. Ruffo et al. developed an AM cost model that estimated different cost drivers for powder based selective laser sintering processes [37]. Other AM cost models and prediction tools have been developed by Lindemann et al. [38, 39], Baumers et al. [17, 40], Dinda et al. [41], and Rickenbacher et al. [42]. In these studies, material usage, build time, laser power, scan speed, hatch spacing, and production volume have all been found to significantly influence production costs.

Despite this work identifying the major factors that drive AM costs, studies that incorporate cost assessment to support DFAM are limited. Yim and Rosen developed an AM selection tool based on cost estimation [43]. Barclift et al. introduced a CAD integrated cost estimation method that provides feedback to the user while they design the parts in a solid modeling program [44]. Yao et al. developed a cost-driven design methodology for AM platforms in product families [45]. These studies guide the selection of different AM techniques based on the lower-cost methods or provide feedback for manual design changes, but none of them offer an optimization approach to select AM designs that minimize production costs.

Process-based cost modeling (PBCM) was developed for assessing the economic performance of new technologies under changing design specifications and manufacturing operations [46]. The method is based on simulating production process parameters (e.g., cycle times, yields, scrap rates) depending on the physical design of a part (e.g., geometry, material selection) and the process design (e.g., manufacturing steps and equipment) to highlight the implications of changing design variables and operating conditions on production costs. PBCM has been applied to analyze the production costs of new technologies or designs such as composite automobile body production [47], electronic semiconductor chip design [48] and optoelectronic transceiver assembly [49]. Laureijs et al. demonstrated the potential of using PBCM for MAM by analyzing the cost competitiveness of an MAM

engine bracket compared to a comparable design produced by forging [50]. Because PBCM is focused on analyzing the production costs associated with alternative design solutions, we chose PBCM as the methodology to account for production costs in a MAM topology optimization in this study.

2.3 Process Mapping

The process variables of MAM machines not only influence the production costs, but also determine the process characteristics (e.g., melt pool dimensions) [51], material microstructure (e.g., grain size, porosity) [52], and material properties (e.g., strength, fatigue) [53,54]. Process and solidification mapping were developed by Gockel et al. [51, 55], Beuth et al. [56, 57], Montogomery et al. [58], and Seifi et al. [53] to predict and control the desired MAM process outcomes through melt pool and microstructure forming through production. The absorbed power and the laser/beam moving speed determines the local cooling rate of the material, which directly influences the melt pool geometry, the grain morphology and grain size. For Ti64 material, studies demonstrate that higher power or lower laser/beam speed leads to larger melt pool area and larger grain size, which reduces the yield strength of the material [59–62]. We use the results of these studies to represent the relationships between MAM process variables and material properties in order to minimize production costs subject to a part's performance constraints.

3 Method

Our design problem aims to find an optimal material distribution inside the design envelope as well as the process parameters to additively manufacture this structure for the minimum production cost. We formulate this problem as a compliance-constrained cost minimization problem

$$\begin{aligned} \underset{\theta}{\text{minimize}} \quad & C(\theta) \\ \text{subject to} \quad & c_0(\theta) \le c_o^{max}(\theta) \\ & \theta_{min} \le \theta \le \theta_{max}. \end{aligned} \quad (1)$$

Here, C is the total production cost and θ is a set of design variables representing the current topology and the process parameters including the beam power and velocity. c_0 is the compliance of the structure for the given parameter set and c_o^{max} represents the maximum allowable compliance.

3.1 Production Cost Model

In order to minimize production cost of MAM processes, a general mathematical representation of MAM production cost is developed based on the typical PBCM approach. We consider production costs that are influenced by structural and/or process variables in two categories: material-based costs and time-based costs [4]. The material-based costs include the material required for printing the part, and material scrap that is lost during powder recovery and recycling. On the other hand, the time-based costs include the

Table 1. Formulation of the constituent factor costs

	Coefficient Description	Unit	Formulation
A_1	Material cost	$\$/mm^3$	$c_m\rho(1-\eta)$
A_2	Manufacturing cost	$\$/h$	$\dfrac{c_{invest}+c_{maintain}L}{LH}+c_{labor}$
A_3	Energy cost	$\$/Wh$	c_{elec}
A_4	Scrap and idle electricity cost	$\$$	$c_m\rho\eta V_{env}+c_{elec}P_0t$

machine cost amortized by the production time necessary to produce the required throughput yield, the energy cost, and the labor cost. We ignore the costs that are not affected by structural or process variables, such as management overhead costs, and thus do not include these cost factors in our cost formulation. Based on the these assumptions, we formulate the total production cost as

$$C = \frac{1}{(1-R)}\left\{A_1V + A_2t + A_3\int_{t_0}^{t} Pdt + A_4\right\}. \quad (2)$$

Here, V is the volume of the part, P is the power required for printing, and t is the total production time required for the part. R is the reject rate representing the percentage of the product rejected due to quality control and destructive testing. A_i's are coefficients that characterize MAM machines and factor input costs such as labor and electricity. Formulations of these coefficients are provided in Table 1 where ρ represents the material density, L is the life time of the machine and H is the annual working time.

The constituent factor costs applied in this cost model—material price, c_m, machine price, c_{invest}, maintenance cost, $c_{maintain}$, labor cost, c_{labor}, energy cost, c_{elec}, and scrap rate, η—are based on the PBCM data presented in [50]. The data are collected from 14 companies for the EBM process with Ti64 material produced in the United States with an annual production volume of 13,500 or greater. The detailed derivation of the cost model is documented in Appendix A.

3.2 Process Mapping

Total required production time is one major driver of production costs in the formulation given in (2). The time is composed of the setup time, sintering time, powder delivery time, and cooling time [17]. For simplicity, we assume that the setup time and cooling time are the same for any print jobs as the geometry has limited influence on these factors. Additionally, we assume that powder delivery time is constant and the same for each layer. Therefore, the production time can be represented as

$$t = t_{build} + t_0 \quad (3)$$

where t_0 is the constant term, and t_{build} varies with the design and process parameters.
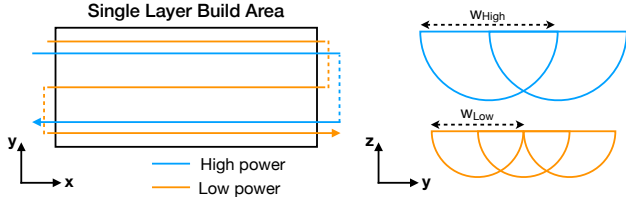
Fig. 2. Influence of beam power on the number of passes (left) and the melt pool size (right). As the beam power is reduced, the melt pool size becomes smaller and consequently a larger number of passes are required to cover the build area. Blue and orange indicates high and low power cases, respectively.
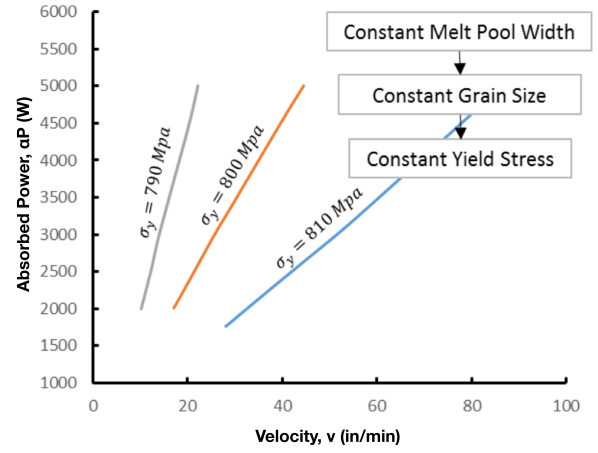

Fig. 3. Demonstration of process mapping of MAM processes for Ti64. The process variables at the same line leads to the same yield strength. Data is obtained from [55].

As discussed in Section 2.3, process-solidification maps have been developed for different MAM processes and can be applied in controlling or predicting melt pool geometry with certain process parameters (e.g., absorbed power, αP, and velocity, v) [51]. The approximate analytical characterization of the process-solidification map can be derived from the Rosenthal equation [63,64]. Following this approach, the melt pool area, A, can be estimated as

$$A = \frac{a_1 \alpha P + a_2}{v} \qquad (4)$$

where a_1 and a_2 are constants that relate to the material and α is the absorption ratio. Here, α is an experimentally determined property [65,66]. Assuming semi-circular melt pool area led by the Rosenthal model [67], the melt pool width, w, can be computed as

$$w = \sqrt{\frac{8A}{\pi}}. \qquad (5)$$

In order to ensure full melting and bonding, we assume half overlap between melt pools in two consecutive passes during the building process (Figure 2). Therefore, the total build time can be formulated as

$$t_{build} = \int N \frac{1}{vh} \, dV_{env} \qquad (6)$$

where $N = 2/w$ represents the number of passes required to cover the unit distance in the y direction, h is the layer thickness and V_{env} is the full building envelope volume. As both speed and power affect the melt pool size directly, they influence the number of passes of the beam that are required to build a single layer. Figure 2 illustrates how beam power affects the number of passes required of the beam path under the same beam velocity.

In addition to the influence it has on production costs, melt pool dimension directly influence the microstructure of a material and thus the mechanical properties of a part. Studies have found that the grain size of Ti64 in MAM is approximately linear to the melt pool width [59], and the yield

strength of the metal is approximately linear to the inverse square root of grain size by the Hall-Petch strengthening relationship [62]. Hence, the yield strength can be formulated as

$$\sigma_y = a_3 \left[\frac{2(a_1 \alpha P + a_2)}{\pi v} \right]^{-\frac{1}{4}} + a_4. \qquad (7)$$

The parameters a_3 and a_4 are experimentally determined coefficients for the specific material. Figure 3 illustrates how the yield strength of the Ti64 material varies with the process parameters (absorbed power, αP, and velocity, v).

3.3 Structure and Process Optimization

In order to find an optimal material distribution, the design envelope is discretized by a volumetric mesh. Similar to topology optimization, each element in the discretized domain is associated with a density variable x_i representing whether element i is full or void. In addition, we assign beam power P_i and velocity v_i to each element to determine the set of process parameters minimizing the overall production cost. Following the modified SIMP method [68], heuristic relationships between the design parameters ($\theta_i = [x_i, P_i, v_i]$) and the element Young's modulus E_i and yield strength Y_i can be given by

$$E_i = E_{min} + x_i^p (E_0 - E_{min}), \qquad (8)$$

$$
\begin{aligned}
Y_i &= Y_{min} + x_i^p (\sigma_y - Y_{min}) \\
&= Y_{min} + x_i^p \left\{ a_3 \left[\frac{2(a_1 \alpha P_i + a_2)}{\pi v_i} \right]^{-\frac{1}{4}} + a_4 - Y_{min} \right\}.
\end{aligned}
\qquad (9)
$$

Here, E_0 represents the Young's modulus of the base material and p is the penalty factor to ensure binary solutions. E_{min}

and Y_{min} are very small elastic modulus and yield strength assigned to the void regions in order to avoid numerical instabilities (e.g. the stiffness matrix becoming singular). The modified SIMP approach improves the classical SIMP method by adding the term E_{min} (and similarly Y_{min} in our case) to prevent zero-stiffness elements and allow the use of straightforward filters [69].

In order to avoid numerical difficulties such as the checkerboard issue [70], we use a basic density filter given in [71] as

$$\tilde{\theta}_i = \frac{\sum_{j \in \mathcal{N}_i} H_{ij} V_j \theta_j}{\sum_{j \in \mathcal{N}_i} H_{ij} V_j}$$
$$\mathcal{N}_i = \{ j : dist(i,j) \le r \},$$
$$H_{ij} = r - dist(i,j)$$

(10)

where $\mathcal{N}_i$ is the neighborhood of element i, r is the filter size, V_j is the volume of element j, H_{ij} is the weight factor, and $\tilde{\theta}_i$ represents the updated design variables. In addition to densities, we use the same filtering approach for power and velocity parameters to avoid drastic changes between neighboring elements.

Using hexagonal elements with size $l_x \times l_y \times l_z$, build time given in (6) can be reformulated in the discretized domain as

$$t_{build} = \sum_i N_i \frac{l_x}{v_i} \frac{l_z}{h}.$$

(11)

Here, we assume that the build direction is z and N_i is the number of passes required to cover in-layer area of the element i. Naively, N_i can be approximated as $N_i = 2l_y/w_i$. However, this approach does not take the element density into consideration and results in artificial increase in power values associated with void elements based on equation (5). To address this problem, we formulate N_i as

$$N_i = 1 + G(x_i) \left(\frac{2l_y}{w_i} - 1 \right)$$

(12)

where $G(x_i) = 1/(1 + e^{(-\kappa(x_i - x_0))})$ is a logistic function that enforces $N_i = 1$ for void elements while keeping $N_i = 2l_y/w_i$ otherwise. For large κ values, the logistic function provides a smooth approximation to the step function while still being differentiable. In this paper, we use $\kappa = 100$ and $x_0 = 0.1$. The cost function in (2) then becomes

$$C(\mathbf{x}, \mathbf{P}, \mathbf{v}) = \frac{1}{(1-R)} \left\{ A_1 l_x l_y l_z \sum_i x_i \right.$$
$$+ A_2 \frac{l_x l_z}{h} \sum_i N_i / v_i$$
$$+ A_3 \frac{l_x l_z}{h} \sum_i P_i N_i / v_i$$
$$\left. + A_4 + A_2 t_0 \right\}.$$

(13)

Similarly, compliance of a structure with material distribution $\mathbf{x}$ can be calculated in the discretized domain as

$$c_o(\mathbf{x}) = \sum_i E_i \mathbf{u}_i^T \mathbf{k_0} \mathbf{u}_i$$

(14)

where $\mathbf{k_0}$ is the element stiffness matrix for an element with unit Young's modulus. We compute the upper bound for the compliance (i.e. the maximum compliance allowed within the candidate structure) as

$$c_o^{max}(\mathbf{x}, \mathbf{P}, \mathbf{v}) = \sum_i \frac{1}{k^2 E_i} V_i \mathbf{Y}_i^T (\mathbf{C_0}^{-1})^T \mathbf{Y}_i$$

(15)

where k is the safety factor, $\mathbf{C_0}$ is the unit constitutive matrix and $\mathbf{Y}_i$ is 6×1 vector of yield strengths. Tensile components of $\mathbf{Y}_i$ are computed using (9) while shear components are assumed to be 50% of the yield strength value according to the maximum shear theory [72] for conservative estimates. Detailed derivation of (15) can be found in the Appendix A.

Optimization Problem Applying (13)-(15) to our optimization formulation (1), the mathematical formulation of the optimization problem can be stated as

$$\begin{aligned} \underset{\mathbf{x}, \mathbf{P}, \mathbf{v}}{\text{minimize}} \quad & C(\mathbf{x}, \mathbf{P}, \mathbf{v}) \\ \text{subject to} \quad & \mathbf{KU} - \mathbf{F} = \mathbf{0}, \\ & V(\mathbf{x})/V_0 - f \le 0, \\ & c_0(\mathbf{x}) - c_o^{max}(\mathbf{x}, \mathbf{P}, \mathbf{v}) \le 0, \\ & 0 \le \mathbf{x} \le 1, \\ & P_{min} \le \mathbf{P} \le P_{max}, \\ & v_{min} \le \mathbf{v} \le v_{max} \end{aligned}$$

(16)

where $\mathbf{U}$ and $\mathbf{F}$ are the global displacement and force vectors and $\mathbf{K}$ is the global stiffness matrix. $\mathbf{x}$, $\mathbf{P}$, $\mathbf{v}$ are the structure and process design variables, specifically density, beam power and velocity, respectively. $V(\mathbf{x})$ and V_0 are the material volume and design domain volume, and f is the prescribed volume fraction. Based on the data provided in [55], we set the limits for power and velocity as $[P_{min}, P_{max}] =$

Table 2. Input parameters to the algorithm

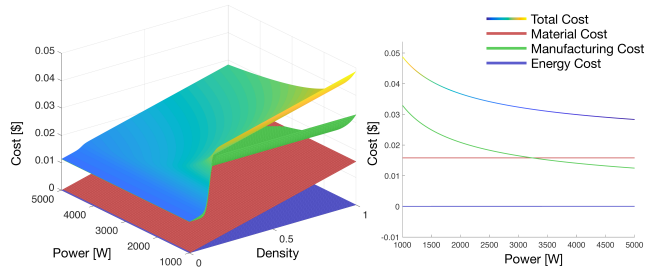| Parameter	Description	Unit	Value
c_m	Material unit cost	$\$/kg$	250
c_{invest}	Machine investment cost	1000\$	1100
$c_{imaintain}$	Maintenance cost	1000\$	50
c_{labor}	Labor unit cost	$\$/h$	26
c_{elect}	Electricity unit cost	$\$/kWh$	0.03
η	Scrap rate	%	1
L	Life time	$year$	7
H	Annual working time	$h/year$	7000
R	Reject rate	%	3.5
α	Absorb ratio	–	0.9
a_1	P-V coefficient	$in^3/Wmin$	0.000302
a_2	P-V coefficient	in^3/min	-0.08941
a_3	Property coefficient	$MPa\,\mu m^{0.5}$	1643.44
a_4	Property coefficient	MPa	772.2
ρ	Density	g/cm^3	4.5
ν	Poisson's ratio	–	0.3
E_0	Young's modulus	GPa	100
E_{min}	Young's modulus of void material	GPa	10^{-9}
Y_{min}	Yield strength of void material	MPa	10^{-6}
p	Penalty factor	–	3
P_0	Idle power	W	2000
h	Layer thickness	mm	0.2

Fig. 4. Change in the production cost with respect to the density and power values for a cubic object with size 2.5mm. The plot on the right illustrates the cost change for $x_i = 1 \ \forall i$.

$[1000, 5000]$ W and $[v_{min}, v_{max}] = [10, 100]$ in/min. It has been reported in the literature that structural defects such as pitting and porosity can be observed for certain scanning speeds and beam power values [73]. Although our formulation does not attempt to resolve such defects directly, the bounds can be arranged to avoid some of these problems during the manufacturing process.

4 Results and Discussion

We demonstrate the developed methodology and the design improvement enabled by the concurrent optimization for EBM process with Ti64 alloy material. Table 2 summarizes the process and material dependent parameters required in the algorithm.

The optimization algorithm is implemented in C++ based on the framework provided by Aage et al. [74]. The framework is modified to incorporate our additional design variables **P** and **v**, cost based objective function and compli-

ance based constraint function. Additionally, we improved the current algorithm to handle free-form 3D geometries. The solution is determined using the method of moving asymptotes (MMA). Derivatives of the objective and constraint functions are analytically derived and incorporated in the algorithm to reduce the computational cost.

4.1 Trade-offs

As the velocity v_i increases, the melt pool width w_i reduces in size, resulting in an increase in the number of passes N_i proportional to $\sqrt{v_i}$ (as formulated in (4)-(5)). On the other hand, time required to complete a single pass decreases linearly with increasing beam velocity. As a result, build time, and consequently the total production cost, are improved. Similarly, yield strength Y_i increases with increasing beam velocity, thereby relaxing the compliance constraint with larger maximum compliance value, c_o^{max}. As the objective and the constraints are not conflicting in v_i in the optimization problem (16), beam velocity needs to be maximized for optimal production cost. For this reason, we set $v_i = v_{max}$ for all elements in the discretized domain and do not optimize the beam velocity for all examples reported in this paper.

Similar to the velocity parameter, increasing power P_i creates a larger melt pool and thus leads to reduction in build time and manufacturing cost because fewer passes are necessary. Conversely, energy cost increases with larger beam power. However, as demonstrated in Figure 4, this increase is very small compared to the change in the manufacturing cost. In addition, larger P_i results in weaker material strength by increasing the grain size (Figure 3). Hence, more material is likely to be necessary to satisfy the compliance constraint. We optimize both the material distribution x_i and the power P_i concurrently to solve these trade-offs for minimum cost MAM.

4.2 Optimization

Figure 5 demonstrates the concurrent optimization results for various 3D design problems. Both density and power distributions are given. In all of the examples, we use $P_i = P_0$ and $x_i = f \ \forall i$ for initialization and we set the volume fraction to be $f = 0.4$. The convergence is obtained in less than 400 iterations for all the examples.

Table 3. Comparison of optimum designs considering different design variables. Columns $[\mathbf{P}|\mathbf{x}]$ and $[\mathbf{x},\mathbf{P}]$ correspond to sequential optimization (first $\mathbf{x}$, then $\mathbf{P}$) and concurrent optimization (ours), respectively.

	Cantilever Beam			L Beam			Bracket			Table		
	$[\mathbf{x}]$	$[\mathbf{P}|\mathbf{x}]$	$[\mathbf{x},\mathbf{P}]$	$[\mathbf{x}]$	$[\mathbf{P}|\mathbf{x}]$	$[\mathbf{x},\mathbf{P}]$	$[\mathbf{x}]$	$[\mathbf{P}|\mathbf{x}]$	$[\mathbf{x},\mathbf{P}]$	$[\mathbf{x}]$	$[\mathbf{P}|\mathbf{x}]$	$[\mathbf{x},\mathbf{P}]$
Build time [h]	2.8	2.6	2.6	33.4	30.1	27.9	8.7	8.2	6.9	8.0	7.3	6.5
Mat. cost [$]	61.7	61.7	60.8	828.3	828.3	828.3	191.8	191.8	193.1	197.0	197.0	197.0
Manuf. cost [$]	154.8	143.5	143.8	1854.2	1673.0	1551.3	482.8	457.9	381.5	446.8	403.4	363.7
Energy cost [$]	0.2	0.2	0.2	2.0	2.4	2.5	0.5	0.6	0.6	0.5	0.6	0.6
Total cost [$]	216.7	205.4	204.8	2684.5	2503.7	2382.1	675.1	650.3	575.2	644.3	601.0	561.3

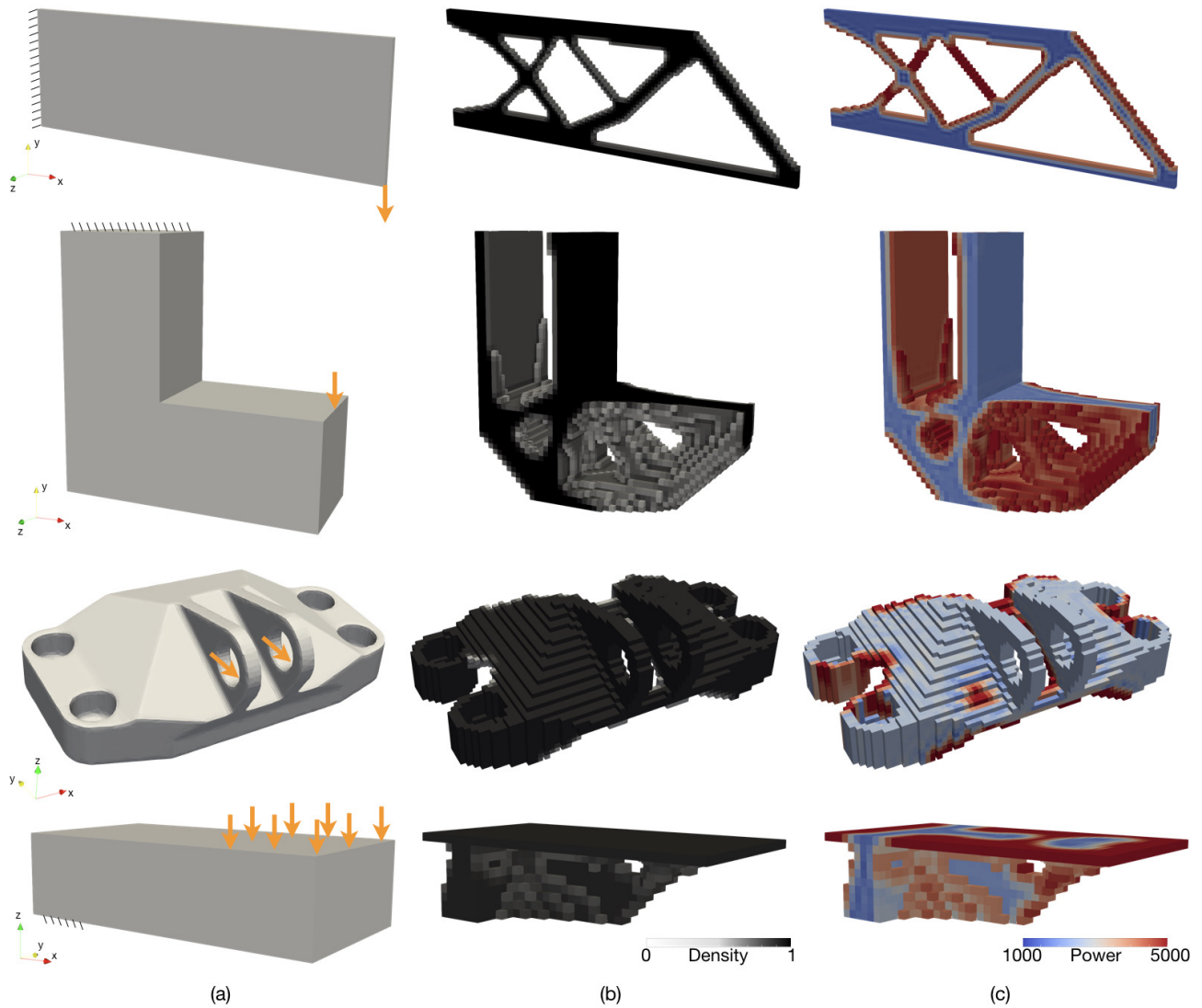|	(a)	(b)	(c)

0 Density 1

1000 Power 5000

Fig. 5. Concurrent optimization results for various problem settings (a). Optimum material and power distributions are given in (b) and (c), respectively. Top to bottom, models are referred to as the cantilever beam, L beam, bracket and table. The bracket model (third row) is fixed to the ground from the four screw holes.

In our solutions, we observe variations in beam power spanning the entire allowable range from P_{min} to P_{max}. High stress regions are assigned lower power values for higher yield strength whereas less critical regions are assigned larger power values to reduce the build time and conse-quently the manufacturing cost as much as possible. Figure 6 illustrates how number of passes N varies for the bracket model on two different slices. Note that smaller number of passes indicates larger scan spacing and shorter build time.
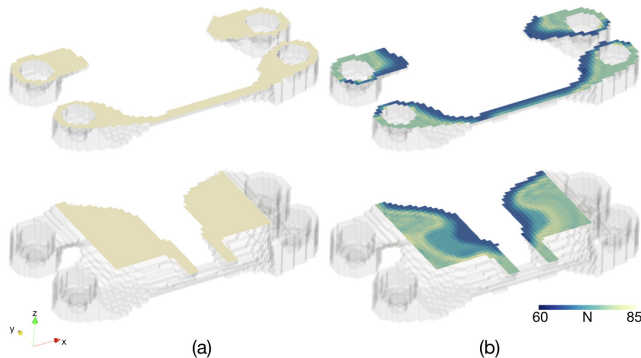
For some applications, users might want to enforce cer-

Fig. 6. Number of passes N computed for two different slices of the optimum bracket designs using (a) $\mathbf{x}$ and (b) $[\mathbf{x}, \mathbf{P}]$ as design variables.

Fig. 7. Comparison of optimum designs using (a) $\mathbf{x}$ and (b) $[\mathbf{x}, \mathbf{P}]$ as design variables. Differences in element densities (i.e. $\mathbf{x}_a - \mathbf{x}_b$) are illustrated in (c).

tain parts of the object to be solid during the optimization, such as screw housings in the bracket model or the top surface of the table. In such situations, our approach allows optimization to keep those regions solid while still reducing the production cost by adjusting the beam power. In the bracket model, it can be observed that certain parts of the screw housings are assigned larger power values to reduce build time and the production cost. Similarly, in the table model, regions of the top surface that do not carry large stresses can be 3D printed faster with larger beam power.

4.3 Comparison
Structural $[\mathbf{x}]$ vs Concurrent $[\mathbf{x}, \mathbf{P}]$ Figure 7 shows the comparison of the optimum designs obtained using two different sets of design variables, $[\mathbf{x}]$ and $[\mathbf{x}, \mathbf{P}]$. In former, we set $\mathbf{P} = P_0$ and in both cases, the objective is set to be the same – total production cost. The solutions in Figure 7(a) are obtained by optimizing the structure only, whereas in Figure 7(b) both the structure and process variables are optimized. As illustrated in Figure 7(c), there are slight differences in how the material is distributed. The difference is more significant in the cantilever beam model where the resulting design includes an additional beam structure at the right corner in the $\mathbf{x}$ only optimization compared to the $[\mathbf{x}, \mathbf{P}]$ design. Such differences in the material distribution result in a compelling decrease in build time (Table 3) by allowing larger power at certain regions and compensating for the resulting decrease in the yield strength.

Further numerical comparisons for various problems are reported in Table 3. The comparisons indicate that concurrent optimization allows further reduction in total production cost by balancing the trade-off between time dependent and material dependent costs. We obtained up to 15% lower total production costs and 21% faster build times with the concurrent optimization compared to optimization that does not consider process variables. It can be observed that the cost improvements are majorly driven by shorter build time, which leads to savings of up to 20% in manufacturing costs. Note that amount of material used might slightly increase in some parts such as the bracket, leading to an increase in material cost compared to the design result from solely opti-
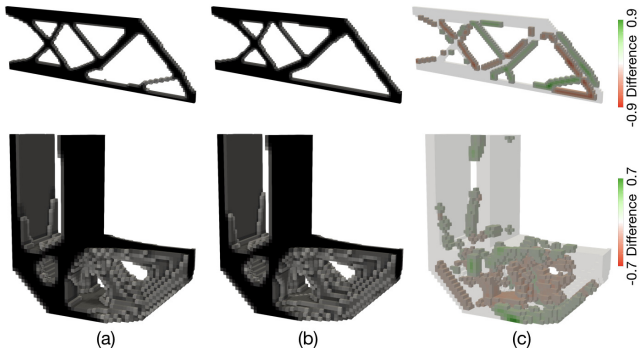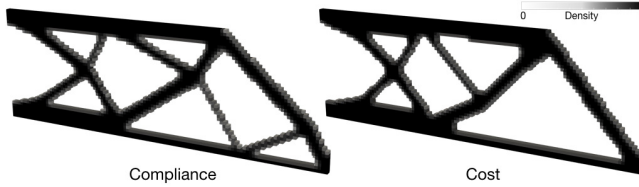
mizing the structure, although total production costs are still lower. The reason behind this is that the cost minimal design is to increase power to reduce the build time. Resulting reduction in compliance is then compensated by adding extra material to certain regions of the part.

The cost savings are sensitive to the unit material cost and the annual operation hours for MAM machines used in the model. The reduction in total MAM production costs obtained by using the concurrent optimization of structural and process variables found in this study is likely a lower bound for the following reasons: (1) Ti64 powder is a relatively expensive material (∼$250/kg) so the cost improvement is likely to be significantly larger for lower cost materials; (2) the annual operating hours (∼7000 hours/year) for the MAM machine is assumed as the maximum suggested by the machine supplier [75], and the cost difference could be larger for cases where annual operating hours are limited to a lower value. In fact, our experiments with the L beam model indicate that cost savings from concurrent optimization increases from 12% to 15% and 14% respectively when the material cost is assumed to be $80/kg and annual operating hours are assumed to be 2000 hours/year as suggested by [76]. Such cost differences could be enough to determine whether AM or conventional manufacturing methods are the most cost-effective option for production of a part [75]. Therefore, the results imply that it may be important to consider process parameters concurrently with a part's structural design when considering whether to manufacture a part with MAM.

Sequential $[\mathbf{P}|\mathbf{x}]$ vs Concurrent $[\mathbf{x}, \mathbf{P}]$ Additionally, we performed a set of experiments to compare performance of our algorithm against a sequential optimization approach. The structure is optimized first and then process variables are optimized. For the initial structural optimization, we set $\mathbf{P} = P_0$ and for sequential power optimization we fix the structure. The objective is set to be the same – total production cost. Expectedly, this kind of a sequential approach performs better than the structure optimization only. However, it is outperformed by our concurrent optimization approach by up to 12% in total production cost and up to 16% in the build time (Table 3).

	Compliance	Cost	Improvement
Build time [h]	2.80	2.58	7.86%
Material cost [$]	60.75	60.75	0.00%
Manuf. cost [$]	155.65	143.84	7.59%
Energy cost [$]	0.17	0.18	-5.55%
Total cost [$]	216.56	204.76	5.45%

Fig. 8. Comparison of optimum designs using compliance and cost as objectives.

Compliance vs Production Cost Objectives We also compare our concurrent optimization approach with the conventional topology optimization for minimum compliance. Figure 8 illustrates the difference between two approaches. Although both approaches use the same amount of material, they converge to solutions with significantly different material distributions. The comparison also demonstrates that using a total production cost model as the objective function results in a ~5% improvement in the overall production cost. For more complicated problem configurations, this improvement can be larger as the build time might play an important role in the resulting cost.

5 Limitations and Future Work

The approach developed in the paper is a proof of concept, and there are several aspects to be improved in the future. Our cost model only considers the economic difference of the manufacturing stage and not other life cycle stages, such as cost benefits brought by light-weighting in the use phase, which may cause changes in the design solutions. Similarly, our cost model does not include post-processing components as required post-processing steps might significantly vary based on functional/geometrical requirements (e.g. geometrical tolerances) and these relationships have not yet been characterized. A natural extension of our approach would be to consider total life cycle costs as well as post-processing costs and their implications in the design solutions. Additionally, our approach does not include optimization of tool path, orientation, packing, production volume, or batch size, which could all be influential factors in the production costs and resulting optimization solutions.

Our cost model assumes that a portion of the unused powder can be recovered and reused in the future prints without any depreciation. We model this using a constant scrap rate parameter. Although our cost model can result in a conservative cost estimate for a large scrap rate, more accurate cost estimates can be obtained using a financial depreciation model for reused metal powders as presented in [77].

In this study, we assume isotropic material properties. For materials with significant anisotropy in their mechanical properties, the final production cost as well as the resulting structure might be inaccurate as the process map could be affected differently in different orientations. Our optimization workflow can easily be extended to cover anisotropy in material properties by modifying the finite element model and the process map accordingly. In the future, the relationship between process variables and material properties could be captured through thermal and microstructure simulations to increase accuracy. In this study, we use a simple first-order approximation to represent this relationship.

6 Conclusion

This paper demonstrates a cost-minimization approach for MAM topology design that concurrently optimizes the structure and process parameters. The approach demonstrates the capability to reduce total production costs by incorporating a process-based cost model into a topology optimization framework. Our formulation including material, labor, energy, and machine costs reveals the trade-offs between these components for varying structure and process parameters. We demonstrate our approach on various 3D geometries for EBM process with Ti64 material using cost estimates from industrial MAM operations. Concurrent optimization of structural design and process parameters is compared against optimization with respect to structural parameters only as well as sequential optimization of structure and process parameters. Results show that more cost effective results can be obtained with similar amount of material by (1) building high stress regions with lower power values to obtain larger yield strength and (2) increasing the power elsewhere to reduce the build time. The results highlight the potential significance of incorporating process design with topology design in order to reduce production costs and build time.

References

[1] Huang, S. H., Liu, P., Mokasdar, A., and Hou, L., 2013. "Additive manufacturing and its societal impact: a literature review". *The International Journal of Advanced Manufacturing Technology,* **67**(5), Jul, pp. 1191–1203.

[2] Huang, R., Riddle, M., Graziano, D., Warren, J., Das, S., Nimbalkar, S., Cresko, J., and Masanet, E., 2016. "Energy and emissions saving potential of additive manufacturing: the case of lightweight aircraft components". *Journal of Cleaner Production,* **135**, pp. 1559 – 1570.

[3] Khajavi, S. H., Partanen, J., and Holmström, J., 2014. "Additive manufacturing in the spare parts supply chain". *Computers in Industry,* **65**(1), pp. 50 – 63.

[4] Thomas, D. S., and Gilbert, S. W., 2014. "Costs and cost effectiveness of additive manufacturing". *NIST Special Publication,* **1176**, p. 12.

[5] Tomlin, M., and Meyer, J., 2011. "Topology optimization of an additive layer manufactured (alm) aerospace part". In Proceeding of the 7th Altair CAE technology conference, pp. 1–9.

[6] Cheng, L., Zhang, P., Biyikli, E., Bai, J., Robbins, J., and To, A., 2017. "Efficient design optimization of variable-density cellular structures for additive manufacturing: theory and experimental validation". *Rapid Prototyping Journal,* **23**(4), pp. 660–677.

[7] Wang, X., Xu, S., Zhou, S., Xu, W., Leary, M., Choong, P., Qian, M., Brandt, M., and Xie, Y. M., 2016. "Topological design and additive manufacturing of porous metals for bone scaffolds and orthopaedic implants: A review". *Biomaterials,* **83**, pp. 127 – 141.

[8] Bendsoe, M. P., and Sigmund, O., 2013. *Topology optimization: theory, methods, and applications.* Springer Science & Business Media.

[9] Eschenauer, H. A., and Olhoff, N., 2001. "Topology optimization of continuum structures: a review". *Applied Mechanics Reviews,* **54**(4), pp. 331–390.

[10] Rozvany, G., 2001. "Aims, scope, methods, history and unified terminology of computer-aided topology optimization in structural mechanics". *Structural and Multidisciplinary Optimization,* **21**(2), Apr, pp. 90–108.

[11] Suzuki, K., and Kikuchi, N., 1991. "A homogenization method for shape and topology optimization". *Computer Methods in Applied Mechanics and Engineering,* **93**(3), pp. 291 – 318.

[12] Rosen, D., 2014. "Design for additive manufacturing: Past, present, and future directions". *Journal of Mechanical Design,* **136**(9), p. 090301.

[13] Doubrovski, Z., Verlinden, J. C., and Geraedts, J. M., 2011. "Optimal design for additive manufacturing: opportunities and challenges". In ASME 2011 International Design Engineering Technical Conferences and Computers and Information in Engineering Conference, American Society of Mechanical Engineers, pp. 635–646.

[14] Zegard, T., and Paulino, G. H., 2016. "Bridging topology optimization and additive manufacturing". *Structural and Multidisciplinary Optimization,* **53**(1), Jan, pp. 175–192.

[15] Gaynor, A. T., Meisel, N. A., Williams, C. B., and Guest, J. K., 2014. "Topology optimization for additive manufacturing: considering maximum overhang constraint". In 15th AIAA/ISSMO multidisciplinary analysis and optimization conference, p. 2036.

[16] Dede, E. M., Joshi, S. N., and Zhou, F., 2015. "Topology optimization, additive layer manufacturing, and experimental testing of an air-cooled heat sink". *Journal of Mechanical Design,* **137**(11), p. 111403.

[17] Baumers, M., Tuck, C., Wildman, R., Ashcroft, I., Rosamond, E., and Hague, R., 2012. "Combined build-time, energy consumption and cost estimation for direct metal laser sintering". In From Proceedings of Twenty Third Annual International Solid Freeform Fabrication Symposium—An Additive Manufacturing Conference, Vol. 13.

[18] Francois, M. M., Sun, A., King, W. E., Henson, N. J., Tourret, D., Bronkhorst, C. A., Carlson, N. N., Newman, C. K., Haut, T., Bakosi, J., et al., 2017. "Modeling of additive manufacturing processes for metals: Challenges and opportunities". *Current Opinion in Solid State and Materials Science,* **21**(LA-UR-16-24513).

[19] Brackett, D., Ashcroft, I., and Hague, R., 2011. "Topology optimization for additive manufacturing". In Proceedings of the solid freeform fabrication symposium, Austin, TX, Vol. 1, pp. 348–362.

[20] Arısoy, Y. M., Criales, L. E., Özel, T., Lane, B., Moylan, S., and Donmez, A., 2017. "Influence of scan strategy and process parameters on microstructure and its optimization in additively manufactured nickel alloy 625 via laser powder bed fusion". *The International Journal of Advanced Manufacturing Technology,* **90**(5), May, pp. 1393–1417.

[21] Aboutaleb, A. M., Bian, L., Elwany, A., Shamsaei, N., Thompson, S. M., and Tapia, G., 2017. "Accelerated process optimization for laser-based additive manufacturing by leveraging similar prior studies". *IISE Transactions,* **49**(1), pp. 31–44.

[22] Martukanitz, R., Michaleris, P., Palmer, T., DebRoy, T., Liu, Z.-K., Otis, R., Heo, T. W., and Chen, L.-Q., 2014. "Toward an integrated computational system for describing the additive manufacturing process for metallic materials". *Additive Manufacturing,* **1-4**, pp. 52 – 63. Inaugural Issue.

[23] Højbjerre, K., 2011. "Additive manufacturing of porous metal components". In Proceedings of the 6th International Conference on Additive Manufacturing, Loughborough.

[24] Mahshid, R., Hansen, H. N., and Højbjerre, K. L., 2016. "Strength analysis and modeling of cellular lattice structures manufactured using selective laser melting for tooling applications". *Materials & Design,* **104**, pp. 276 – 283.

[25] Ponche, R., Hascoet, J., Kerbrat, O., and Mognol, P., 2012. "A new global approach to design for additive manufacturing". *Virtual and Physical Prototyping,* **7**(2), pp. 93–105.

[26] Ulu, N. G., Coros, S., and Kara, L. B., 2018. "Designing coupling behaviors using compliant shape optimization". *Computer-Aided Design,* **101**, pp. 57 – 71.

[27] Bendsøe, M. P., and Kikuchi, N., 1988. "Generating optimal topologies in structural design using a homogenization method". *Computer methods in applied mechanics and engineering,* **71**(2), pp. 197–224.

[28] Ulu, E., Mccann, J., and Kara, L. B., 2017. "Lightweight structure design under force location uncertainty". *ACM Trans. Graph.,* **36**(4), July, pp. 158:1–158:13.

[29] Gardan, N., and Schneider, A., 2015. "Topological optimization of internal patterns and support in additive manufacturing". *Journal of Manufacturing Systems,*

37, pp. 417 – 425.

[30] Chu, C., Graf, G., and Rosen, D. W., 2008. "Design for additive manufacturing of cellular structures". *Computer-Aided Design and Applications,* **5**(5), pp. 686–696.

[31] Bendsøe, M. P., 1989. "Optimal shape design as a material distribution problem". *Structural optimization,* **1**(4), pp. 193–202.

[32] Rozvany, G. I. N., Zhou, M., and Birker, T., 1992. "Generalized shape optimization without homogenization". *Structural optimization,* **4**(3), Sep, pp. 250–252.

[33] Ulu, E., Korkmaz, E., Yay, K., Ozdoganlar, O. B., and Kara, L. B., 2015. "Enhancing the structural performance of additively manufactured objects through build orientation optimization". *Journal of Mechanical Design,* **137**(11), p. 111410.

[34] Hopkinson, N., and Dicknes, P., 2003. "Analysis of rapid manufacturing—using layer manufacturing processes for production". *Proceedings of the Institution of Mechanical Engineers, Part C: Journal of Mechanical Engineering Science,* **217**(1), pp. 31–39.

[35] Previtali, B., Demir, A. G., Bucconi, M., Crosato, A., and Penasa, M., 2017. "Comparative costs of additive manufacturing vs. machining: The case study of the production of forming dies for tube bending". In 28th Annual International Solid Freeform Fabrication Symposium–An Additive Manufacturing Conference. Austin Texas USA 7th-9th August.

[36] Auth, C., Arndt, A., and Anderl, R., 2017. "Method for the evaluation of economic efficiency of additive and conventional manufacturing". In 28th Annual International Solid Freeform Fabrication Symposium–An Additive Manufacturing Conference. Austin Texas USA 7th-9th August.

[37] Ruffo, M., Tuck, C., and Hague, R., 2006. "Cost estimation for rapid manufacturing - laser sintering production for low to medium volumes". *Proceedings of the Institution of Mechanical Engineers, Part B: Journal of Engineering Manufacture,* **220**(9), pp. 1417–1427.

[38] Lindemann, C., Jahnke, U., Moi, M., and Koch, R., 2012. "Analyzing product lifecycle costs for a better understanding of cost drivers in additive manufacturing". In 23th Annual International Solid Freeform Fabrication Symposium–An Additive Manufacturing Conference. Austin Texas USA 6th-8th August.

[39] Lindemann, C., Jahnke, U., Moi, M., and Koch, R., 2013. "Impact and influence factors of additive manufacturing on product lifecycle costs". In Solid Freeform Fabrication Symposium, University of Texas, Austin, TX, pp. 998–1009.

[40] Baumers, M., Dickens, P., Tuck, C., and Hague, R., 2016. "The cost of additive manufacturing: machine productivity, economies of scale and technology-push". *Technological Forecasting and Social Change,* **102**, pp. 193 – 201.

[41] Dinda, S., Modi, D., Simpson, T., Tedia, S., and Williams, C., 2017. "Expediting build time, material, and cost estimation for material extrusion processes to enable mobile applications". In 43rd Design Automation Conference, Vol. 2A-2017, American Society of Mechanical Engineers (ASME).

[42] Rickenbacher, L., Spierings, A., and Wegener, K., 2013. "An integrated cost-model for selective laser melting (slm)". *Rapid Prototyping Journal,* **19**(3), pp. 208–214.

[43] Yim, S., and Rosen, D., 2012. "Build time and cost models for additive manufacturing process selection". In ASME 2012 International Design Engineering Technical Conferences and Computers and Information in Engineering Conference, American Society of Mechanical Engineers, pp. 375–382.

[44] Barclift, M., Armstrong, A., Simpson, T., and Joshi, S., 2017. "Cad-integrated cost estimation and build orientation optimization to support design for metal additive manufacturing". In 43rd Design Automation Conference, Vol. 2A-2017, American Society of Mechanical Engineers (ASME).

[45] Yao, X., Moon, S. K., and Bi, G., 2016. "A cost-driven design methodology for additive manufactured variable platforms in product families". *Journal of Mechanical Design,* **138**(4), p. 041701.

[46] Busch, J. V., and Field III, F. R., 1988. "Technical cost modeling". *Blow Molding Handbook*, pp. 839–871.

[47] Fuchs, E. R., Field, F. R., Roth, R., and Kirchain, R. E., 2008. "Strategic materials selection in the automobile body: Economic opportunities for polymer composite design". *Composites Science and Technology,* **68**(9), pp. 1989 – 2002.

[48] Marallo, S. L., and Dieffenbach, J., 1994. "Manufacturing cost analysis for electronic packaging". In Economics of Design, Test, and Manufacturing, 1994. Proceedings., Third International Conference on the, IEEE, p. 90.

[49] Fuchs, E. R., Bruce, E., Ram, R., and Kirchain, R. E., 2006. "Process-based cost modeling of photonics manufacture: the cost competitiveness of monolithic integration of a 1550-nm dfb laser and an electroabsorptive modulator on an inp platform". *Journal of lightwave technology,* **24**(8), p. 3175.

[50] Laureijs, R. E., Roca, J. B., Narra, S. P., Montgomery, C., Beuth, J. L., and Fuchs, E. R., 2017. "Metal additive manufacturing: Cost competitive beyond low volumes". *Journal of Manufacturing Science and Engineering,* **139**(8), p. 081010.

[51] Gockel, J., Beuth, J., and Taminger, K., 2014. "Integrated control of solidification microstructure and melt pool dimensions in electron beam wire feed additive manufacturing of ti-6al-4v". *Additive Manufacturing,* **1-4**, pp. 119 – 126. Inaugural Issue.

[52] Cunningham, R., Narra, S. P., Ozturk, T., Beuth, J., and Rollett, A. D., 2016. "Evaluating the effect of processing parameters on porosity in electron beam melted ti-6al-4v via synchrotron x-ray microtomography". *JOM,* **68**(3), Mar, pp. 765–771.

[53] Seifi, M., Christiansen, D., Beuth, J., Harrysson, O.,

and Lewandowski, J. J., 2016. "Process mapping, fracture and fatigue behavior of ti-6al-4v produced by ebm additive manufacturing". In Proceedings of the 13th World Conference on Titanium, John Wiley & Sons, Inc., pp. 1373–1377.

[54] Lewandowski, J. J., and Seifi, M., 2016. "Metal additive manufacturing: a review of mechanical properties". *Annual Review of Materials Research, **46**,* pp. 151–186.

[55] Gockel, J., and Beuth, J., 2013. "Understanding ti-6al-4v microstructure control in additive manufacturing via process maps". In Solid Freeform Fabrication Symposium, University of Texas, Austin, TX, pp. 12–14.

[56] Beuth, J., Fox, J., Gockel, J., Montgomery, C., Yang, R., Qiao, H., Soylemez, E., Reeseewatt, P., Anvari, A., Narra, S., et al., 2013. "Process mapping for qualification across multiple direct metal additive manufacturing processes". In Proceedings of SFF Symposium., Austin, TX, Aug, pp. 12–14.

[57] Beuth, J., and Klingbeil, N., 2001. "The role of process variables in laser-based direct metal solid freeform fabrication". *JOM, **53**(9),* Sep, pp. 36–39.

[58] Montgomery, C., Beuth, J., Sheridan, L., and Klingbeil, N., 2015. "Process mapping of inconel 625 in laser powder bed additive manufacturing". In Solid Freeform Fabrication Symposium, pp. 1195–1204.

[59] Xu, W., Brandt, M., Sun, S., Elambasseril, J., Liu, Q., Latham, K., Xia, K., and Qian, M., 2015. "Additive manufacturing of strong and ductile ti–6al–4v by selective laser melting via in situ martensite decomposition". *Acta Materialia, **85**,* pp. 74 – 84.

[60] Sergueeva, A., Stolyarov, V., Valiev, R., and Mukherjee, A., 2001. "Advanced mechanical properties of pure titanium with ultrafine grained structure". *Scripta Materialia, **45**(7),* pp. 747 – 752.

[61] Leuders, S., Vollmer, M., Brenne, F., Tröster, T., and Niendorf, T., 2015. "Fatigue strength prediction for titanium alloy tial6v4 manufactured by selective laser melting". *Metallurgical and Materials Transactions A, **46**(9),* Sep, pp. 3816–3823.

[62] Callister, W. D., and Rethwisch, D. G., 2011. *Materials science and engineering*, Vol. 5. John Wiley & Sons NY.

[63] Tang, M., and Pistorius, P. C., 2017. "Anisotropic mechanical behavior of alsi10mg parts produced by selective laser melting". *JOM, **69**(3),* Mar, pp. 516–522.

[64] Rosenthal, D., 1941. "Mathematical theory of heat distribution during welding and cutting". *Welding journal, **20**,* pp. 220s–234s.

[65] Zhou, B., Zhou, J., Li, H., and Lin, F., 2017. "Fabrication and characterization of ti6al4v by selective electron beam and laser hybrid melting". In 28th Annual International Solid Freeform Fabrication Symposium–An Additive Manufacturing Conference. Austin Texas USA 7th-9th August.

[66] Trapp, J., Rubenchik, A. M., Guss, G., and Matthews, M. J., 2017. "In situ absorptivity measurements of metallic powders during laser powder-bed fusion additive manufacturing". *Applied Materials Today, **9**,* pp. 341 – 349.

[67] Soylemez, E., Beuth, J. L., and Taminger, K., 2010. "Controlling melt pool dimensions over a wide range of material deposition rates in electron beam additive manufacturing". In Proceedings of 21st Solid Freeform Fabrication Symposium, Austin, TX, Aug, pp. 9–11.

[68] Andreassen, E., Clausen, A., Schevenels, M., Lazarov, B. S., and Sigmund, O., 2011. "Efficient topology optimization in matlab using 88 lines of code". *Structural and Multidisciplinary Optimization, **43**(1),* Jan, pp. 1–16.

[69] Sigmund, O., 2007. "Morphology-based black and white filters for topology optimization". *Structural and Multidisciplinary Optimization, **33**(4),* Apr, pp. 401–424.

[70] Bonnetier, E., and Jouve, F., 1998. "Checkerboard instabilities in topological shape optimization algorithms". In Proceedings of the Conference on Inverse Problems, Control and Shape Optimization PICOF, Vol. 98.

[71] Liu, K., and Tovar, A., 2014. "An efficient 3d topology optimization code written in matlab". *Structural and Multidisciplinary Optimization, **50**(6),* Dec, pp. 1175–1196.

[72] Shigley, J. E., Budynas, R. G., and Mischke, C. R., 2004. *Mechanical engineering design.* McGraw-Hill.

[73] Wang, X., Gong, X., and Chou, K., 2015. "Scanning speed effect on mechanical properties of ti-6al-4v alloy processed by electron beam additive manufacturing". *Procedia Manufacturing, **1**,* pp. 287–295.

[74] Aage, N., Andreassen, E., and Lazarov, B. S., 2015. "Topology optimization using petsc: An easy-to-use, fully parallel, open source topology optimization framework". *Structural and Multidisciplinary Optimization, **51**(3),* Mar, pp. 565–572.

[75] Atzeni, E., and Salmi, A., 2012. "Economics of additive manufacturing for end-usable metal parts". *The International Journal of Advanced Manufacturing Technology, **62**(9),* Oct, pp. 1147–1155.

[76] Allen, J., 2006. An investigation into the comparative costs of additive manufacture vs. machine from solid for aero engine parts. Tech. rep., Rolls-Royce PLC Derby, UK.

[77] Barclift, M., Joshi, S., Simpson, T., and Dickman, C., 2016. "Cost modeling and depreciation for reused powder feedstock in powder bed fusion additive manufacturing". In Proceedings of the 27th annual international solid freeform fabrication symposium. Austin, TX, USA.

Appendix A: Derivations of Cost and Allowable Compliance Equations

Production Cost   We break the production cost into material based costs and time based costs. The material based costs include the material required for printing the design of the part and material scrap that is lost during powder recov-

ery and recycling. The time based costs include the machine cost allocated to the production time, the energy cost and other costs depending on the production time such as labor cost.

$$C = \frac{1}{(1-R)}(C_{mat} + C_{time})$$
$$= \frac{1}{(1-R)}(C_{mat,part} + C_{mat,waste} \qquad (17)$$
$$+ C_{time,machine} + C_{time,labor} + C_{time,energy})$$

where $C_{mat,part}$ is the material cost of the part, $C_{mat,waste}$ is the cost of the waste material, $C_{time,machine}$ is the amortized cost of the AM machine, $C_{time,labor}$ is the cost of labor, and $C_{time,energy}$ is the cost of energy. Individual components of the cost can be formulated as

$$C_{mat,part} = c_m \rho V$$
$$C_{mat,waste} = c_m \rho \eta (V_{env} - V)$$
$$C_{time,machine} = c_{mach} t = \frac{c_{invest} + c_{maintain} L}{LH} t \qquad (18)$$
$$C_{time,labor} = c_{labor} t$$
$$C_{time,energy} = \int_{t_0}^{t} c_{elec}(P + P_0) dt$$

where descriptions of the parameters and values used in this work is reported in Table 2. The cost formulation can be further reduced to

$$C = \frac{1}{(1-R)}\left\{ c_m \rho V + c_m \rho \eta (V_{env} - V) \right.$$
$$+ \frac{c_{invest} + c_{maintain} L}{LH} t + c_{labor} t$$
$$\left. + \int_{t_0}^{t} c_{elec}(P + P_0) dt \right\}$$
$$= \frac{1}{(1-R)}\left\{ c_m \rho (1 - \eta) V \qquad (19) \right.$$
$$+ \left(\frac{c_{invest} + c_{maintain} L}{LH} + c_{labor} \right) t$$
$$\left. + c_{elec} \int_{t_0}^{t} P dt + c_m \rho \eta V_{env} + c_{elec} P_0 t \right\}$$
$$= \frac{1}{(1-R)}\left\{ A_1 V + A_2 t + A_3 \int_{t_0}^{t} P dt + A_4 \right\}.$$

Allowable Compliance The maximum compliance of the structure is derived as

$$c_o^{max}(\mathbf{x}, \mathbf{P}, \mathbf{v}) = \sum_i E_i \mathbf{u}_i^T \mathbf{k_0} \mathbf{u}_i$$
$$= \sum_i E_i \mathbf{u}_i^T (V_i \mathbf{B}_i^T \mathbf{C_0} \mathbf{B}_i) \mathbf{u}_i$$
$$= \sum_i E_i V_i (\mathbf{u}_i^T \mathbf{B}_i^T) \mathbf{C_0} (\mathbf{B}_i \mathbf{u}_i)$$
$$= \sum_i E_i V_i (E_i^{-1} \mathbf{C_0}^{-1} \sigma_i)^T \mathbf{C_0} (E_i^{-1} \mathbf{C_0}^{-1} \sigma_i)$$
$$= \sum_i \frac{1}{E_i} V_i \sigma_i^T (\mathbf{C_0}^{-1})^T \sigma_i$$
$$\leq \sum_i \frac{1}{E_i} V_i \frac{1}{k} \mathbf{Y}_i^T (\mathbf{C_0}^{-1})^T \frac{1}{k} \mathbf{Y}_i$$
$$= \sum_i \frac{1}{k^2 E_i} V_i \mathbf{Y}_i^T (\mathbf{C_0}^{-1})^T \mathbf{Y}_i$$
$$(20)$$

where $\mathbf{Y}_i = [Y_i, \; Y_i, \; Y_i, \; Y_i/2, \; Y_i/2, \; Y_i/2]^T$ and Y_i is given in (9).